

1 Supplementary Material for:

2 **Source characterization of the 20<sup>th</sup> May 2024  $M_D$  4.4 Campi Flegrei caldera earthquake**  
3 **through a joint source-propagation probabilistic inversion**

4

5 M. Supino<sup>1\*</sup>, L. Scognamiglio<sup>1</sup>, L. Chiaraluce<sup>1</sup>, C. Doglioni<sup>1</sup>, A. Herrero<sup>1</sup>

6

7 <sup>1</sup>Istituto Nazionale di Geofisica e Vulcanologia, Roma, Italy.

8

9

10 *List of content:*

11 Texts S1 to S2

12 Figures S1 to S2

13

## Text S1. Pre-processing and processing parameters

We select a 3-second S-wave time window for the inversion, starting 0.1 s before the S-wave arrival time. We then follow the signal and spectrum pre-processing described in Supino et al. (2019). The main steps are the following: (1) We remove constant and linear trend from the signal, and then apply a Hann-function tapering on the first and last 5% of the data. (2) We obtain the S-wave spectrum computing FFT of the pre-processed signal. The displacement amplitude spectrum ( $\Omega_0$ ) is smoothed with a 5-point moving average filter, and finally converted to seismic moment units ( $M_0$ ) according to the following equation (Aki & Richards, 1980):

$$M_0 = \Omega_0 \cdot \frac{1}{\xi} = \Omega_0 \cdot \frac{4\pi \cdot \rho \cdot v_S^3 \cdot r_H}{R_{\theta\phi} \cdot F_S} \quad (S1)$$

where  $\rho$  is the propagation medium density,  $v_S$  is the S-wave velocity,  $r_H$  is the hypocentral distance,  $R_{\theta\phi}$  is the radiation pattern coefficient and  $F_S$  is the free-surface coefficient.

We used  $\rho = 2500 \text{ kg m}^{-3}$  (Judenherc & Zollo, 2004),  $v_S = 1685 \text{ m s}^{-1}$  (Orsi et al., 1999),  $R_{\theta\phi} = 0.63$  (Aki & Richards, 1980; Boore & Boatwright, 1984),  $F_S = 2$ . The values assigned to the parameters are similar to those considered by Petrosino et al. (2008) for the study region.

The hypocentral distance  $r_H$  has been computed for each station assuming the INGV-OV event location (latitude = 40.8277°N, longitude = 14.138°E, depth = 2.6 km).

The frequency band used for the inversion is 0.2 – 40 Hz. For each station we invert a single spectrum  $\log \tilde{u}(f)$ , with  $\tilde{u}(f)$  geometric mean of the displacement amplitude spectra of the two horizontal components. The forward operator used for the inversion is the same as defined in Supino et al. (2019), eq. (4):

$$g(\mathbf{m} = (M_0, f_c, \gamma, Q'); f) = \log M_0 - \log \left[ 1 + \left( \frac{f}{f_c} \right)^\gamma \right] + \log \xi - \log e \cdot \pi \frac{r_H}{v_S} f \cdot Q' \quad (S2)$$

with  $M_0$  (seismic moment),  $f_c$  (corner frequency),  $\gamma$  (high-frequency decay exponent) source parameters of a generalized Brune (1970) spectral model,  $Q' = 1/Q + k_0 \cdot v_S/r_H$  with  $Q$  anelastic attenuation quality factor and  $k_0$  site-dependent attenuation term (Anderson & Hough, 1984), and  $\xi, v_S, r_H$  as in eq. S1.

We do not consider a site amplification term in the forward operator, since the inversion is performed on a single event while a set of events is needed to constrain site amplification. Nevertheless, the large number of stations used to obtain the averaged event source parameters is expected to mitigate possible site amplification effects, if any.

The probabilistic framework used to estimate the joint a-posteriori PDF  $\sigma(\mathbf{m})$  is the same as defined in Supino et al. (2019), based on the work by Tarantola (2005), with the hypothesis of a uniform a-priori PDF over the model space, and of modelization and data uncertainties normally distributed (see Section 3.1 and eqs. 5,6 in Supino et al. (2019) for details).

## Test S2. P-waves inversion

We inverted P-waves using the same methodology and parameters described for S-wave inversions, changing the following values according to the selected phase:  $v_P = 3000 \text{ m s}^{-1}$  (Orsi et al., 1999),  $R_{\theta\phi} = 0.52$  (Aki & Richards, 1980; Boore & Boatwright, 1984), and inverting the vertical component spectrum.

49 We obtained  $M_w = 3.55 \pm 0.06$  selecting a 1-second time window, and  $M_w = 3.79 \pm 0.06$  selecting a 1.5-second  
50 time window.

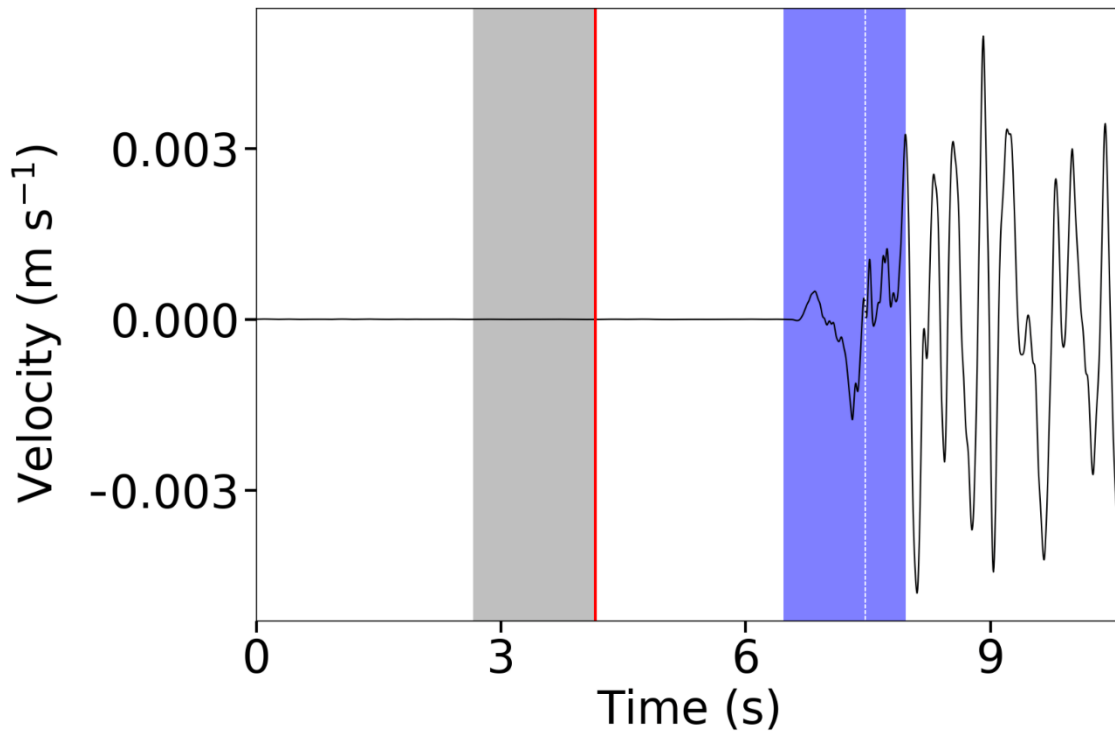
51 As we show in Figure S1, with the 1.5-second time window we selected part of the S-wave, while the 1-second  
52 time window was not enough to include the whole P-phase. This is the observational reason why the two  $M_w$   
53 values obtained for the two P-wave inversions probably represent an underestimation and an overestimation of  
54 the moment magnitude for the earthquake.

55

## 56 References

- 57 Aki, K., & Richards, P. G. (1980). Quantitative Seismology, Theory and Methods Volume I and Volume II. In  
58 *Book* (Vol. 68, Issue 5).
- 59 Anderson, J. G., & Hough, S. E. (1984). A model for the shape of the Fourier amplitude spectrum of  
60 acceleration at high frequencies. *Bulletin of the Seismological Society of America*, 74(5), 1969–1993.  
61 <https://doi.org/10.1785/BSSA0740051969>
- 62 Boore, D. M., & Boatwright, J. (1984). Average body-wave radiation coefficients. *Bulletin of the Seismological*  
63 *Society of America*, 74(5), 1615–1621. <https://doi.org/10.1785/BSSA0740051615>
- 64 Brune, J. N. (1970). Tectonic stress and the spectra of seismic shear waves from earthquakes. *Journal of*  
65 *Geophysical Research*, 75(26), 4997–5009. <https://doi.org/10.1029/JB075i026p04997>
- 66 Judenherc, S., & Zollo, A. (2004). The Bay of Naples (southern Italy): Constraints on the volcanic structures  
67 inferred from a dense seismic survey. *Journal of Geophysical Research: Solid Earth*, 109(B10).  
68 <https://doi.org/10.1029/2003JB002876>
- 69 Kaneko, Y., & Shearer, P. M. (2014). Seismic source spectra and estimated stress drop derived from cohesive-  
70 zone models of circular subshear rupture. *Geophysical Journal International*, 197(2), 1002–1015.  
71 <https://doi.org/10.1093/gji/ggu030>
- 72 Madariaga, R. (1976). Dynamics of an expanding circular fault. *Bull. Seismol. Soc. Am.*
- 73 Orsi, G., Civetta, L., Del Gaudio, C., de Vita, S., Di Vito, M. A., Isaia, R., Petrazzuoli, S. M., Ricciardi, G. P.,  
74 & Ricco, C. (1999). Short-term ground deformations and seismicity in the resurgent Campi Flegrei caldera  
75 (Italy): an example of active block-resurgence in a densely populated area. *Journal of Volcanology and*  
76 *Geothermal Research*, 91(2–4), 415–451. [https://doi.org/10.1016/S0377-0273\(99\)00050-5](https://doi.org/10.1016/S0377-0273(99)00050-5)
- 77 Petrosino, S., De Siena, L., & Del Pezzo, E. (2008). Recalibration of the Magnitude Scales at Campi Flegrei,  
78 Italy, on the Basis of Measured Path and Site and Transfer Functions. *Bulletin of the Seismological Society*  
79 *of America*, 98(4), 1964–1974. <https://doi.org/10.1785/0120070131>
- 80 Supino, M., Festa, G., & Zollo, A. (2019). A probabilistic method for the estimation of earthquake source  
81 parameters from spectral inversion: application to the 2016–2017 Central Italy seismic sequence.  
82 *Geophysical Journal International*, 218(2), 988–1007. <https://doi.org/10.1093/gji/ggz206>
- 83 Tarantola, A. (2005). Inverse Problem Theory and Methods for Model Parameter Estimation. In *Inverse*  
84 *Problem Theory and Methods for Model Parameter Estimation*. Society for Industrial and Applied  
85 Mathematics. <https://doi.org/10.1137/1.9780898717921>

86

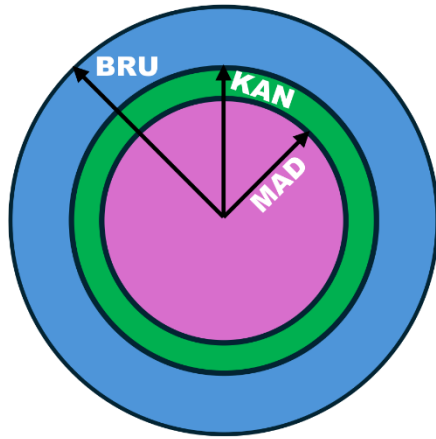


87

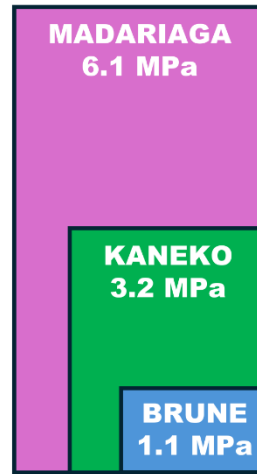
88 **Figure S1.** 1.5-second P-wave time window (blue rectangle). The red vertical line shows the origin time of the  
89 earthquake. The white dotted vertical line indicates 1-second after the start of the time window. Station CMIS,  
90 vertical component.

91

### SOURCE DIMENSION



### STRESS DROP



92

93

94

**Figure S2.** Visual comparison between source dimension and stress drop estimated assuming Brune (1970), Kaneko and Shearer (2014) and Madariaga (1976) model.